Growth of rutile TiO_2 thin films on Pt/TiO_2/SiO_2/Si (SSTOP) substrate for resistive random access memory (ReRAM) device application

Mabkhoot A. Alsaiari,[a,b*] Nabil A. Alhemiary[a] and Ahmad Umar[b]

[a]Department of Chemistry, Faculty of Science and Arts, Sharurah Branch, Najran University, Najran, Kingdom of Saudi Arabia

[b]Promising Centre for Sensors and Electronic Devices, Najran University, Kingdom of Saudi Arabia

***All correspondence should be addressed:**

Email: mamalsaiari@nu.edu.sa

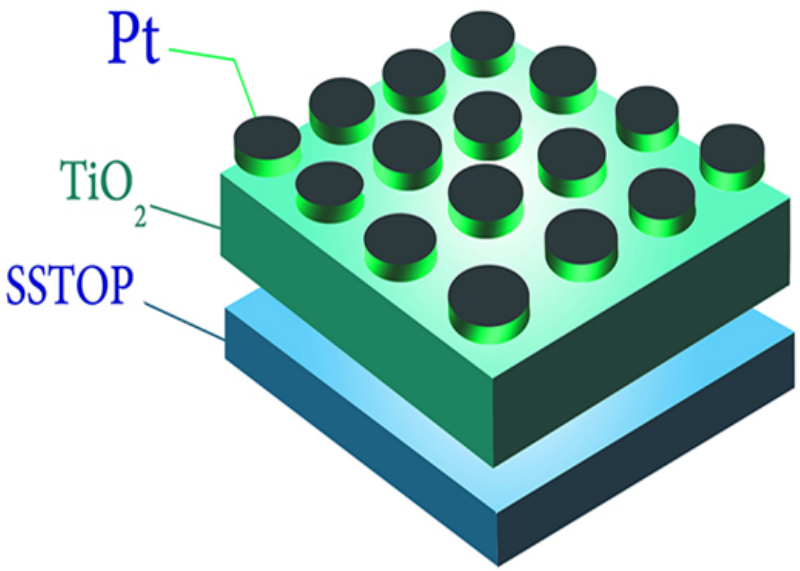

Graphical Abstract. Design for ReRAM device based on Pt/TiO_2/SiO_2/Si (SSTOP) substrate

ABSTRACT

Memory structures play a basic role in providing integrated circuits of powerful processing capabilities. Even most powerful processors have nothing to offer without an accompanying memory and importantly, the development of mobile devices is dependent on the continual improvement of memory technology. Herein, we report the synthesis of TiO_2 thin films on SSTOP (Pt/TiO2/SiO2/Si) substrate via physical vapor deposition process for the first time. The layers consisted of Si, SiO_2, TiO_2 and Pt, hence the SSTOP shorthand is used throughout the text. Three different phases of TiO_2 thin films were obtained, i.e. amorphous, anatase and rutile phases, by controlling the reaction parameters. The deposited films were examined by scanning electron microscopy (SEM), energy dispersive spectroscopy (EDS) and Raman Spectroscopy in order to understand the crystallographic, morphological, compositional and scattering properties. The grown thin films on SSTOP substrates were further utilized for the fabrication of resistive random access memory (ReRAM) devices. The initial electrical screening was performed on capacitor-like structures which were prepared using platinum top electrodes (diameter = 250 μm) on a 14x14 array metal contact mask. Current-Voltage (I-V) measurements were implemented employing a range of current compliances (IC).

Keywords: *Combinatorial synthesis; TiO_2; resistive switching (RS); non-volatile ReRAM*

1. INTRODUCTION

Combinatorial chemistry and high throughput (HT) methods have emerged during the last decade due to the challenge of developing materials for different applications [1]. These techniques aid in the design and rapid synthesis of a variety of material libraries, and they allow the screening of libraries in a rapid sequential or parallel manner. Combinatorial methods have been successfully applied to resistive random access memory (ReRAM) using CVD[1]. Combinatorial libraries with a high level of control in composition gradient thin films can also be achieved over the simultaneous deposition of multiple elements through evaporation. This approach has been used in the development of phase change random access memory (PCRAM) materials [2].

Metal oxides play an important role in ReRAM mechanisms [3-7] with the archetypical system based on phases of Titania. It was observed that the titania phases (doped and un-doped) can be combinatorial synthesized when combining metal elemental evaporation with a plasma atom source[8]. We have extended this approach to the synthesis and screening of materials and devices for ReRAM. A range of ReRAM fabrication methods have been reported in the literature [9-15]. They usually involve a combination of the following deposition techniques: pulsed laser deposition (PLD) [9], thermal oxidation and low pressure chemical vapour deposition (CVD) [10], photolithography and reactive ion etching [11], electron-gun evaporation under high vacuum [12], RF magnetron sputtering at room temperature under a low oxygen

environment [13], RF coupled with DC magnetron sputtering or thermal evaporation, atomic layer deposition (ALD) [14] and rapid thermal annealing (RTA) [15]. A common limitation of the fabrication methods described in the literature is that they only allow for the synthesis of a defined composition and thickness of the TMO layer at a time. Additionally, the involvements of various instruments at each step are relatively complicated, time-consuming and costly process which represents a drawback of the materials design and optimization of ReRAMs.

Many materials have been tested for ReRAM application, among these resistive switching materials, binary metal oxides are of great interest, especially TiO_2, the most commonly reported oxide in ReRAM. TiO_2 has been studied as a high-k capacitor oxide [12]. It is intrinsically an insulator, meaning it has a very high resistance. The conductivity of film occurs by making the oxide richer with oxygen vacancies, which behave like positively charged species. By applying an external voltage bias in a stoichiometry film, it is possible to drift the oxygen vacancies. In addition, due to the simplicity of its fabrication, ReRAM shows both unipolar and bipolar RS, which makes it easier to study both mechanisms [16]. Moreover, TiO_2 is compatible with CMOS, a cheap, non-toxic material, and is chemically stable; its electrical properties, on the other hand, are unstable, which leads to either more insulation or conduction through the appropriate choice of impurities [17]. TiO_2 is widely used in different areas of research under various forms, such as single crystals and ceramics, or as thin films, such as optical application [18] and photocatalysis [19]. TiO_2 is also used as a support material due to its

high conductivity in the sub-stoichiometric or doped form [20]. Because of such interesting properties and numerous applications, titanium dioxide has been chosen as a benchmark material for this high-throughput research in order to establish a reliable screening of ReRAM material.

Thus, in this paper we report the synthesis of TiO_2 thin films on SSTOP (Pt/TiO2/SiO2/Si) substrate via physical vapor deposition process for the first time. Three different phases of TiO_2 thin films were obtained, i.e. amorphous, anatase and rutile phases, by controlling the reaction parameters and the grown thin films on SSTOP substrates were further utilized for the fabrication of resistive random access memory (ReRAM) devices.

2. EXPERIMENTAL DETAILS

2.1. Growth of TiO_2 thin films on SSTOP substrate

A range of metal oxide thin films of TiO_2 were prepared on 28mm × 28mm platinized Si-substrate. Titanium deposition was carried out using an electron beam source combined with a plasma atom source to achieve the titania phases. Such preparation methods are described in detail elsewhere [8 ,21]. These films were prepared with a constant chamber pressure of $2.5x10^{-5}$ mBar at 5 sccm oxygen flow rate and plasma source power of *rf*= 400W, in order to obtain stoichiometric oxides. Titania films of ca.

250 nm were prepared (confirmed by profiler meters), and the phases were controlled through the substrate deposition temperature and post processing [8].

2.2. Characterizations of the TiO_2 thin films grown on SSTOP substrate

X-ray diffraction (XRD) patterns were recorded on a Rigaku smart lab 9KW SN JD3604N. The X-rays were generated by a Cu-Kα source with the wavelength of 1.54 Å. The scans passed through a specified 2θ range by moving the detection and X-ray source, both. All measurements were done at a grazing incidence angle of 1°. A typical 2θ range was between 10° and 60°. Samples deposited on SSTOP substrates were positioned on a stage with X-Y-Z control. Keysight Technologies 5600LS Atomic Force Microscope was used for AFM characterizations. Measurements of film thickness were carried out in tapping mode using a Nanosensors Point probe-Plus n-doped Si tip with a resonant frequency range of 146 kHz to 236 kHz. The thin films topography was measured over a space of approximately 50 μm at a 0:5 lines/s scan rate and a resolution of 512 points/line. The proportional and integral gain parameters of the feedback loop had to be adjusted manually for each measurement point.

Room-temperature Raman-scattering spectra were collected using an XPLORA confocal Raman microscope (Horiba Jobin Yvon, Inc.) coupled to Olympus BX41 optical microscope. The spectrometer was equipped with a 532-nm, 25-mW solid-state laser. The spot size of the laser on the samples was approximately 1 μm. The experiment was repeated three times on each sample in order to obtain a good signal and confirm the

expected phase. The laser power was kept sufficiently low in order to minimize any localized heating of the material

SEM/EDS measurements were performed by JEOL JSM-5910 scanning electron microscope, fitted with an Oxford Instruments x-act 51-ADD0006 EDS silicon drift detector. The Oxford Inca 300 EDS software was used for analysis. The composition of top electrode and oxide before and after the electrical test was achieved by means of EDS coupled with SEM. Samples that were tested electrically were introduced into the analysis chamber and placed under vacuum. The working distance of the measurement was 10 mm, with a magnification of 500x and accelerating voltage of 12V.

3. Results and Discussion

3.1. Characterizations and properties of TiO_2 thin films grown over SSTOP substrate

X-ray diffraction (XRD) analysis was used to identify the crystalline property of grown TiO_2 films on SSTOP substrate. Three different phases, i.e. amorphous, anatase and rutile phases were obtained for the grown TiO_2 thin films. **Figure 1(a)** shows the deposited titania film on the SSTOP substrate at a 5-sccm oxygen flow rate, a plasma source of P*rf* = 400 W and a deposition rate of 4 Å/s. It was noticed that the titania was in the amorphous phase. Two methods were followed to grow the crystalline titania thin films samples. First, for thicker titania films (150 nm–300 nm), the sample (**Figure 1(b)**) was deposited at room temperature, followed by annealing for 1h at 450 °C under an oxygen atmosphere in a tube furnace to obtain anatase phase. However, the other

sample (**Figure 1(c)**) was prepared by deposition of TiO_2 at a substrate temperature of 600 ˚C, followed by annealing for 1h at 600 °C under an oxygen atmosphere in a tube furnace to obtain rutile phase. Second, thinner TiO_2 samples (10–60 nm) were annealed after deposition inside the chamber for 1h at 200 ˚C under a flow rate of 1 sccm of oxygen to produce an anatase structure. Alternatively, the rutile was annealed at 1100 °C in a tube furnace for 2h under an oxygen atmosphere. All diffraction peaks were identified.

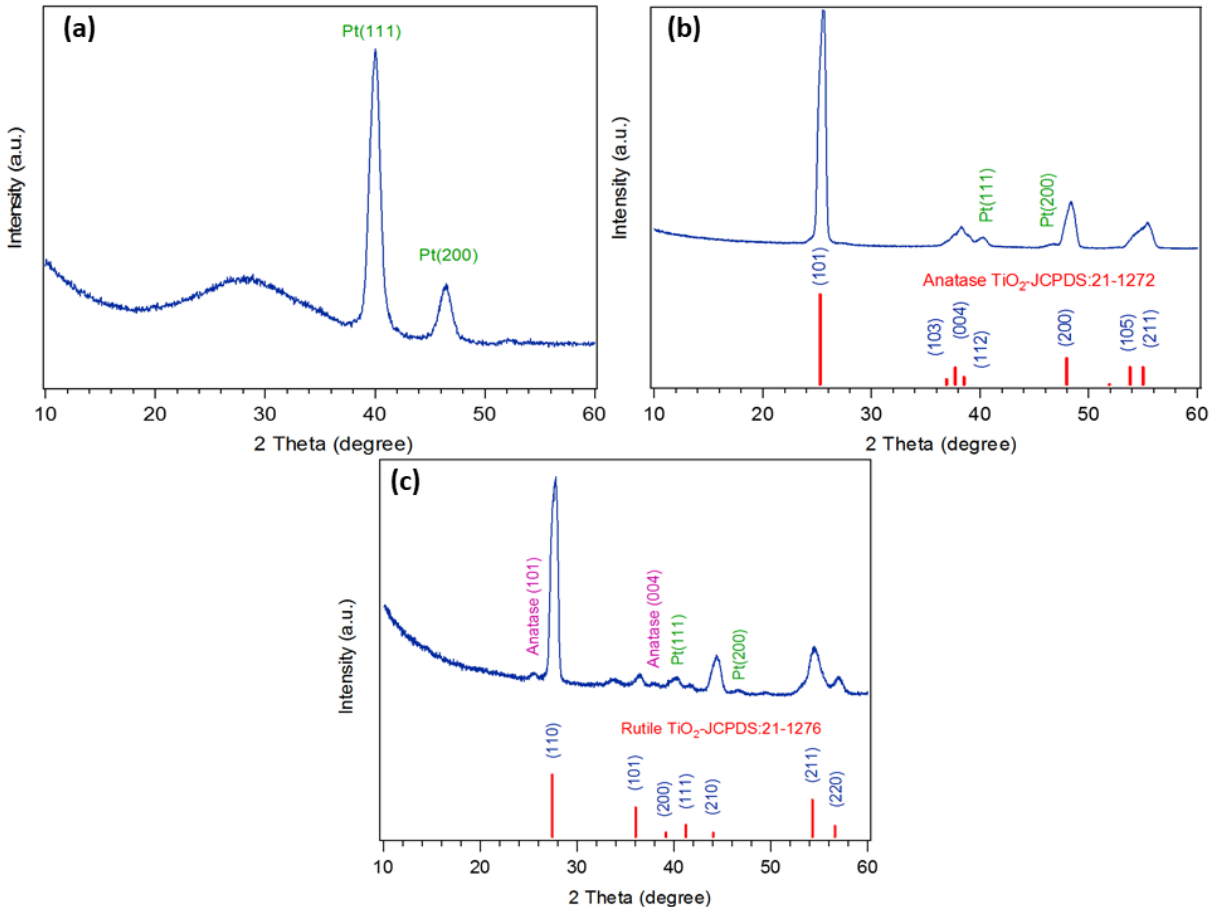

Figure 1: Typical XRD patterns of (a) as-grown TiO_2 film, (b) TiO_2 film annealed at 450℃ (anatase phase), and (c) TiO_2 film deposited at 600 ℃ using an atomic oxygen plasma source.

Figure 1(b) depicts the typical XRD characterization for the TiO_2 film annealed at 450℃. Interestingly various peaks related with anatase phase TiO_2 were observed in the

pattern which confirmed the formation of anatase phase of TiO_2 thin film. The appearance of two peaks on the SSTOP substrate corresponding to Pt can be observed at 2θ= 40° and 46°, respectively. The XRD pattern of TiO_2 film deposited at 600 ℃ using an atomic oxygen plasma source is shown in **figure 1 (c)** which clearly confirmed the formation of rutile phase of TiO_2 thin film. Some very short peaks related with anatase phase of TiO2 were also seen in the observed XRD pattern.

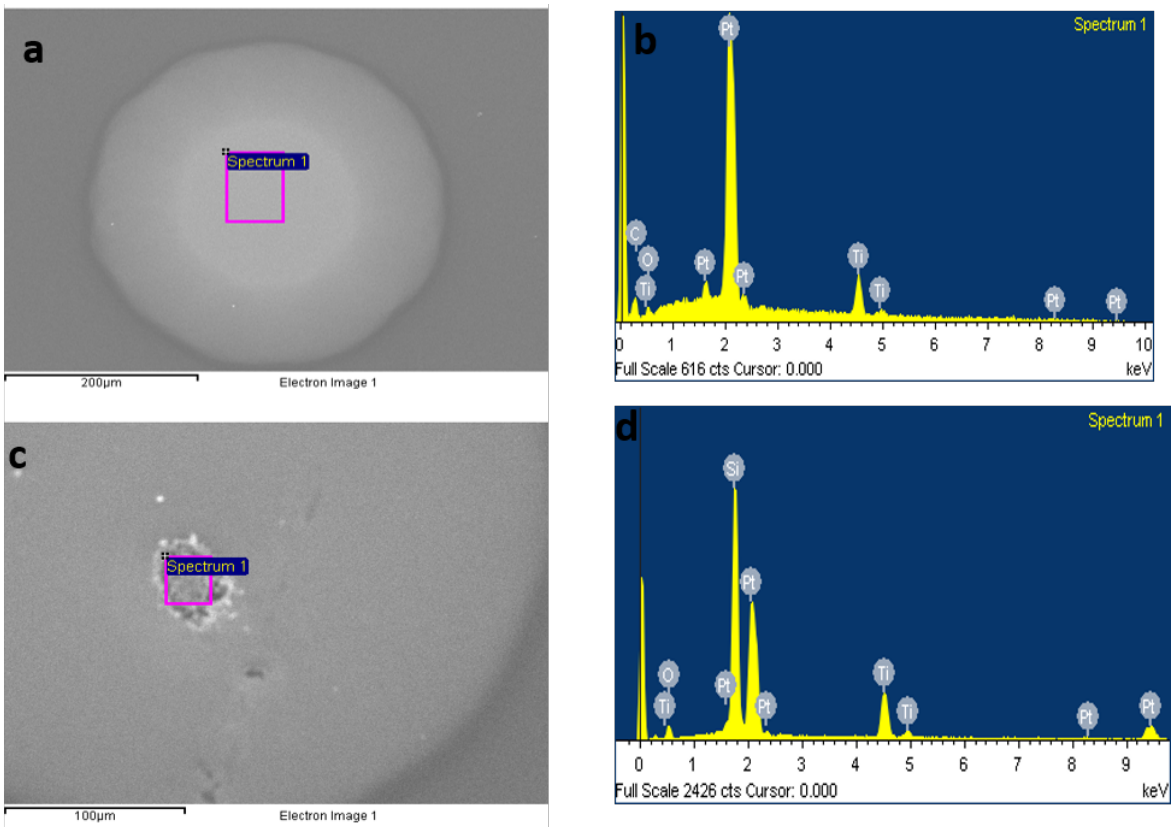

Figure 2. (A) SEM topography of a Pt top electrode before an electrical test, (B) signal of Pt before an electrical test, (C) top electrode after an electrical test, and (D) signal of Pt after an electrical test.

The scanning electron microscopic (SEM) images of Pt/TiO_2/Pt capacitor-like structure and their corresponding energy dispersive X-ray spectroscopy (EDX) analysis were done before and after the dielectric breakdown (formation process) and shown in

figure 2. The SEM images clearly revealed that before an electrical test, the Pt surfaces were clean and smooth (**figure 2 (a)**), however, after the dielectric breakdown, many holes were formed on the surface of the Pt, which partially destroyed the electrode as well as the TiO_2 layer (**figure 2 (c)**). Interestingly, the EDX analysis indicated that the Pt signal was lowered and Si signal was sharply enhanced after breakdown (**Figure 2(d)**) compared to prior of electrical test (**Figure 2(b)**). Such phenomenon confirmed that the Pt was nearly peeled off in the outer circle.

Atomic force microscopy (AFM) was taken for different phases of TiO_2 to observe the surface properties of the grown thin films and obtained results are presented in **figure 3**. Interestingly, it was observed that the surface morphologies of the grown TiO_2 thin films were changed according to the growth temperature. With increasing the deposition temperature, the surfaces of the grown thin films were changed from flatter (amorphous, figure 3 (a)) to the rough surfaces for anatase and rutile phases (figure 3 (b) and (c)).

Raman scattering spectroscopy was used to confirm the synthesized TiO_2 phases. **Figure 4** shows the Raman spectra of the synthesized thin films in three different phases, i.e. amorphous, anatase and rutile. The amorphous phase is characterized by no vibrational features however, the anatase phase has five Raman active modes (at 162, 210, 414, 533, 519 and 657 cm^{-1}) and rutile has three Raman active mode (162, 460 and 632 cm^{-1}). The observed scattering peaks are well consistent with the reported literature [22-24].

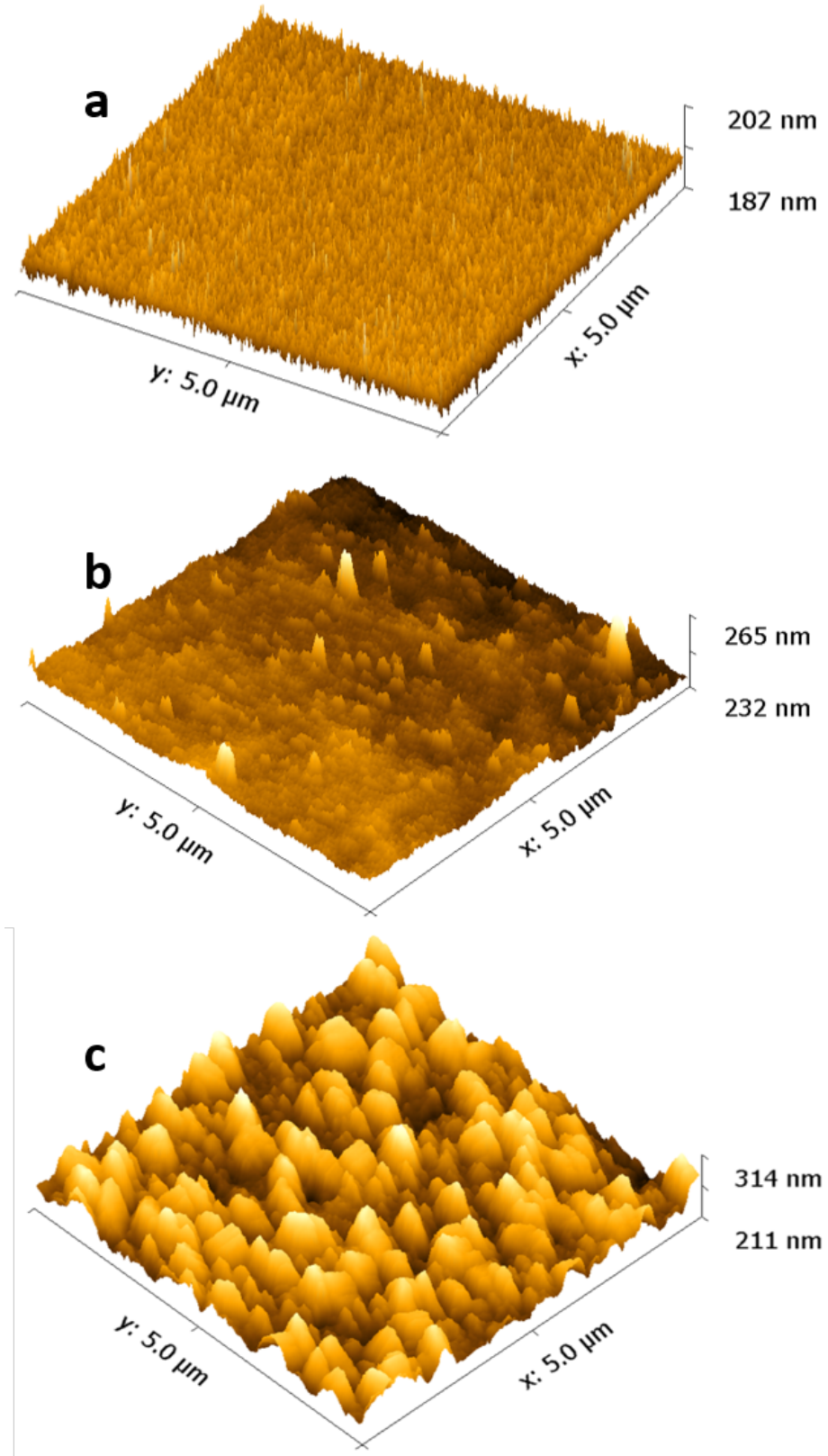

Figure 3. AFM topography of three phases of TiO_2 (a), (b) and (c) belong to amorphous, anatase and rutile, respectively.

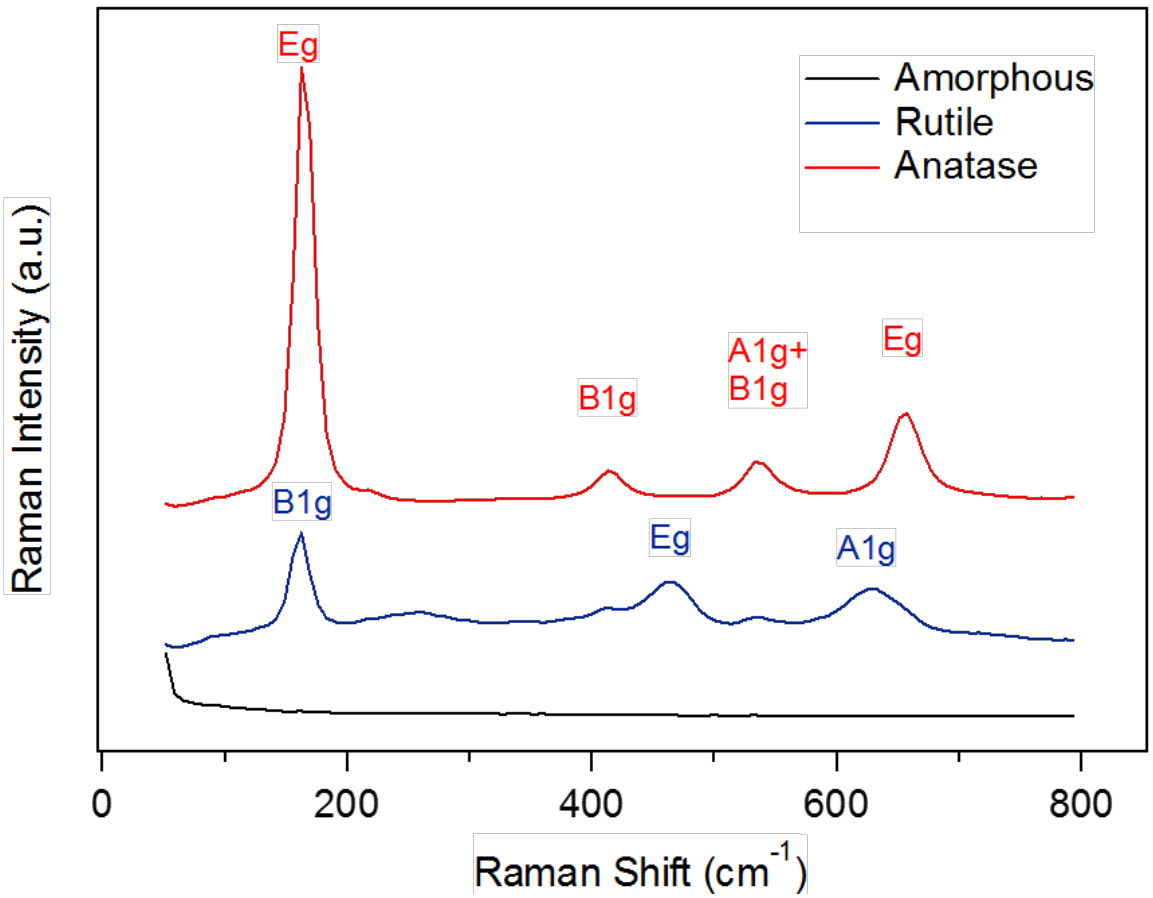

Figure 4. Raman-scattering spectra of three TiO_2 phases with average thickness of (270 nm) synthesis using HT-PVD.

3.2. ReRAM application of TiO_2 thin films grown over SSTOP substrate

The I-V sweeps were conducted using direct current measurement (DC) that used to determine $V_{Forming}$ and switching voltage for the prepared titania thin films. All measurements were performed using a B1500A Semiconductor Device Analyzer in corporation with probe station. Parametric tests were performed on titania deposited on platinized silicon substrates. These substrates consisted of a series of layers on top of which a 100 nm-thick Pt layer was deposited. The layers consisted of Si, SiO_2, TiO_2 and

Pt, hence the SSTOP shorthand is used throughout the text. The conductive Pt layer functioned as a bottom contact onto which a probe was connected.

***Characteristics of the Pt/ TiO_2/ Pt Device*:**

Pt/TiO_2/Pt structures of three phases (amorphous, anatase and rutile) were swept with a positive/negative voltage on the top electrodes, while the bottom electrodes were grounded, and then swept back to zero. At the beginning, all devices were swept to a high voltage (E > 3.5 V), as it was believed that the step required higher voltage for the 'forming process' [25-27] and then the subsequent voltage was decreased. The diameter of the circular-shaped top electrode (TE) was 250 μm. The thickness of all devices presented in this paper was 50 nm. The unipolar switching behavior took place regardless of the polarity of the applied voltage, meaning that SET and RESET processes can be achieved under both positive and negative voltages, whereas bipolar behavior was found to depend on the voltage polarity.

a) Pt/ amorphous TiO_2/ Pt

The devices were swept to positive voltage and then swept back to zero. The IC in all forming measurements was constant (1 mA) (**Figure 5**). It is worth noting that in every measurement, read voltage was applied in the initial state (**Figure 5(b)**); then, the voltage was increased slowly until the device switched. Since this took place at different voltages, the maximum voltage of the sweep varied. For amorphous titania, the voltage

was swept to 6 V and there was an increase in the current at 5.1 V, with a sudden jump in current observed at around 5.45 V, at which point the device formed (**Figure. 5(a)**): A conductive path was created between the top and bottom electrode through the oxide, and the device remained in the conductive state (ON) as the voltage was swept back to zero. The read voltage after this forming step was obtained (**Figure. 5(c)**).

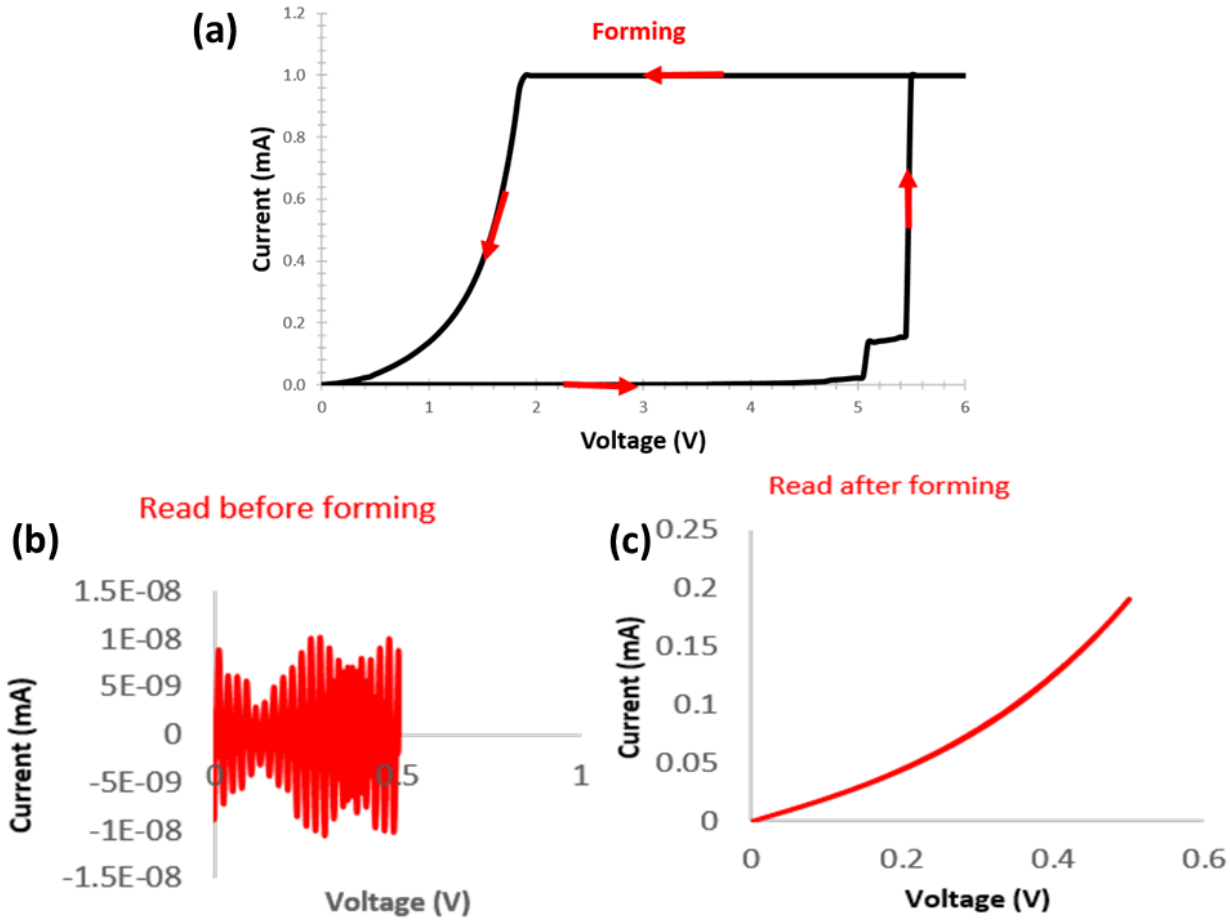

Figure 5. **(a)** Forming process of amorphous titania. Initial state (as-prepared sample), and (b) read before forming, (c) read after forming. (Thickness 50nm).

After forming the device (LRS), the IC value was set higher (double) than that for the forming process, and the voltage swept with the same polarity: A RESET process

took place at 0.75 V (**Figure 6 (a)**), where the conductive path was apparently disconnected, and the device returned to the HRS (OFF). The voltage was swept again with the same polarity using the same IC of the forming step (1 mA), at which the device switch at 1.4 V from the HRS to the LRS (**Figure 6 (b)**) (this is a lower voltage than that required in the forming process), where the conductive path reconnected.

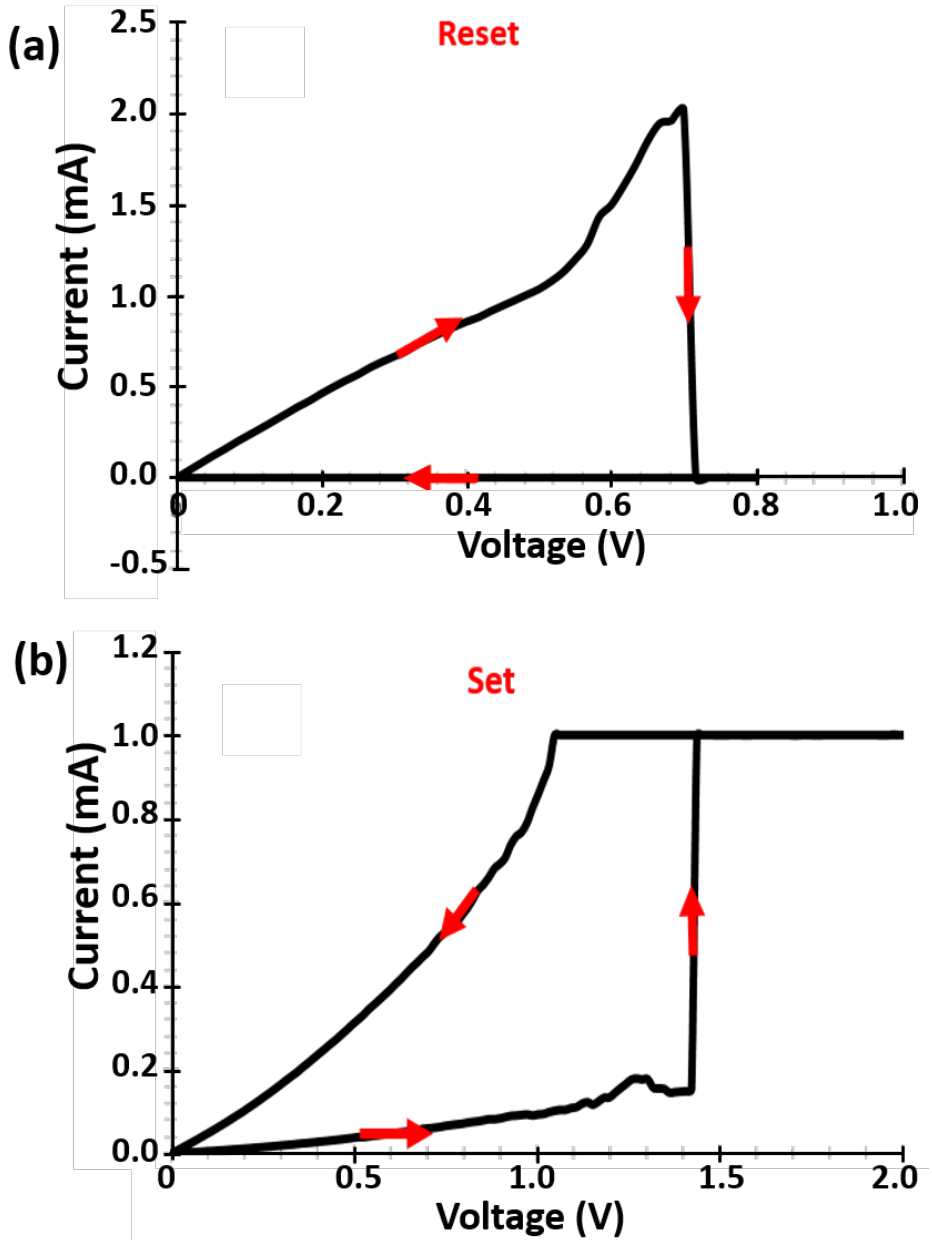

Figure 6. Sweeps of unipolar resistive switching behaviour of amorphous titania. (A) reset process and (B) set process. (Thickness 50nm).

b) Pt/Crystalline TiO_2/Pt

The same test strategy was followed for crystalline titania (both anatase and rutile phases). For anatase, the voltage was swept in a positive direction at which the device had high resistance. However, at 5.2 V, there was a gradual increase of the current, and conductivity increased until 7.1 V, where a sudden jump of current was observed and the device was formed, as shown in **Figure 7(a)**. The device switched from irreversible state IRS (HRS) to LRS. Read voltages were taken before and after the FS, as displayed in **Figure 7(b) and (c)**.

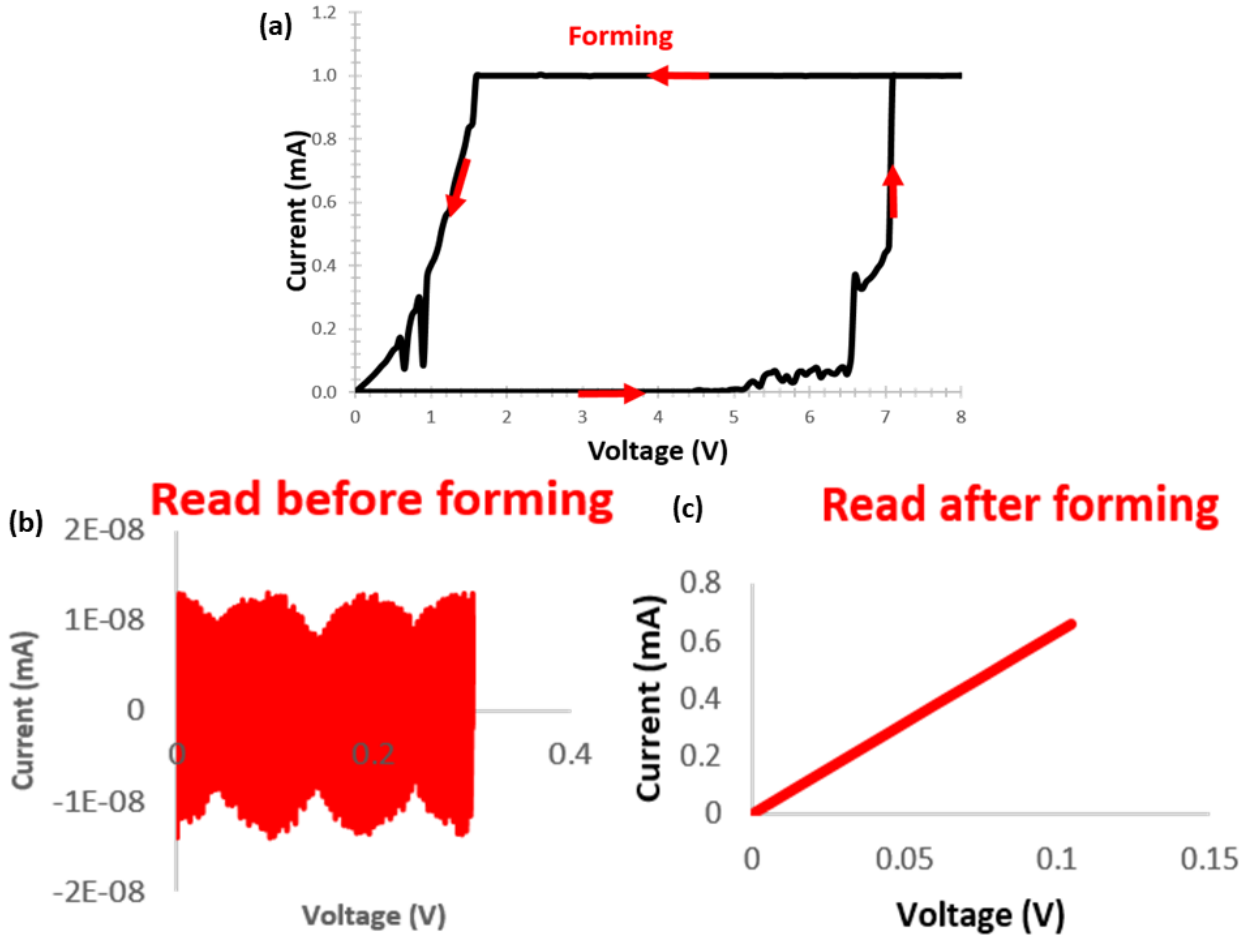

Figure 7. **(a)** Forming process of anatase titania. (b) Read before and (c) after forming. (Thickness 50 nm).

After setting IC to a higher target than the forming process (8 mA), the voltage was swept to 1.5 V, where it switched to 1.3 V from LRS to HRS (reset process), at which point the conductive path was broken (**Figure 8(a)**). The voltage was swept again in order to set the device from HRS to LRS on the same polarity where the switching took place at 3.4 V, as shown in **Figure 8 (b)**.

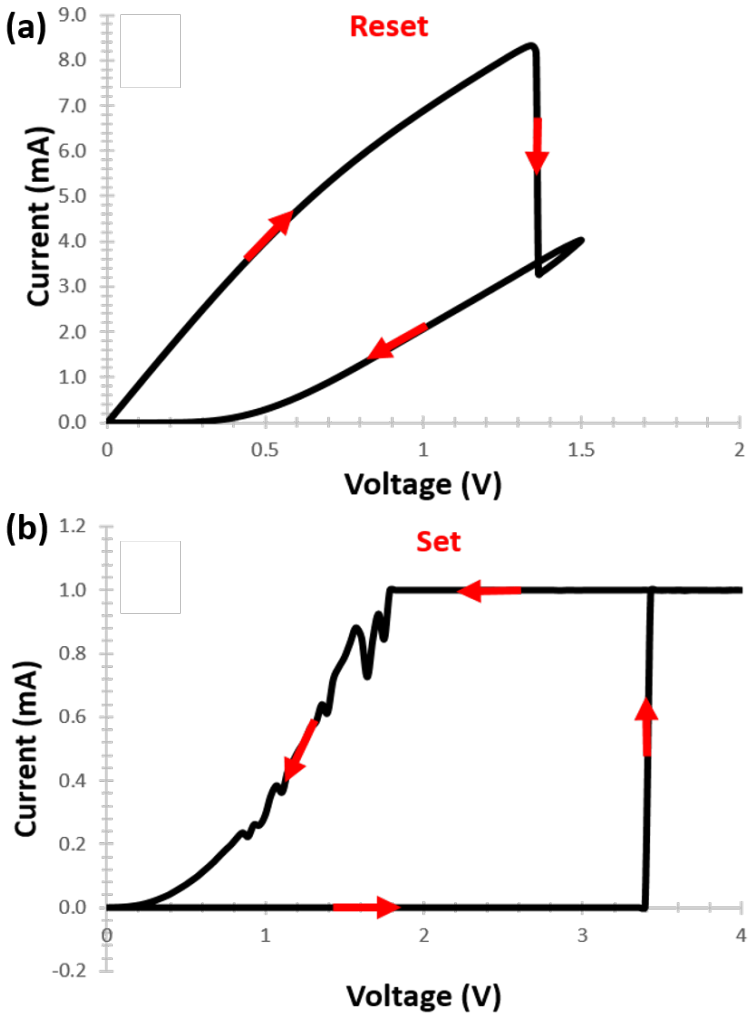

Figure 8. Sweeps of unipolar resistive switching behaviour of anatase titania. (A) reset process, and (B) set process. (Thickness 50nm).

Rutile titania was formed at 9.4 V (**Figure 9(a)**), at which point it was in a very high resistance state, as shown in read voltage before forming (**Figure 9(b)**) at an IC of 1 mA. Read voltage after forming is displayed in **Figure 9 (c)**.

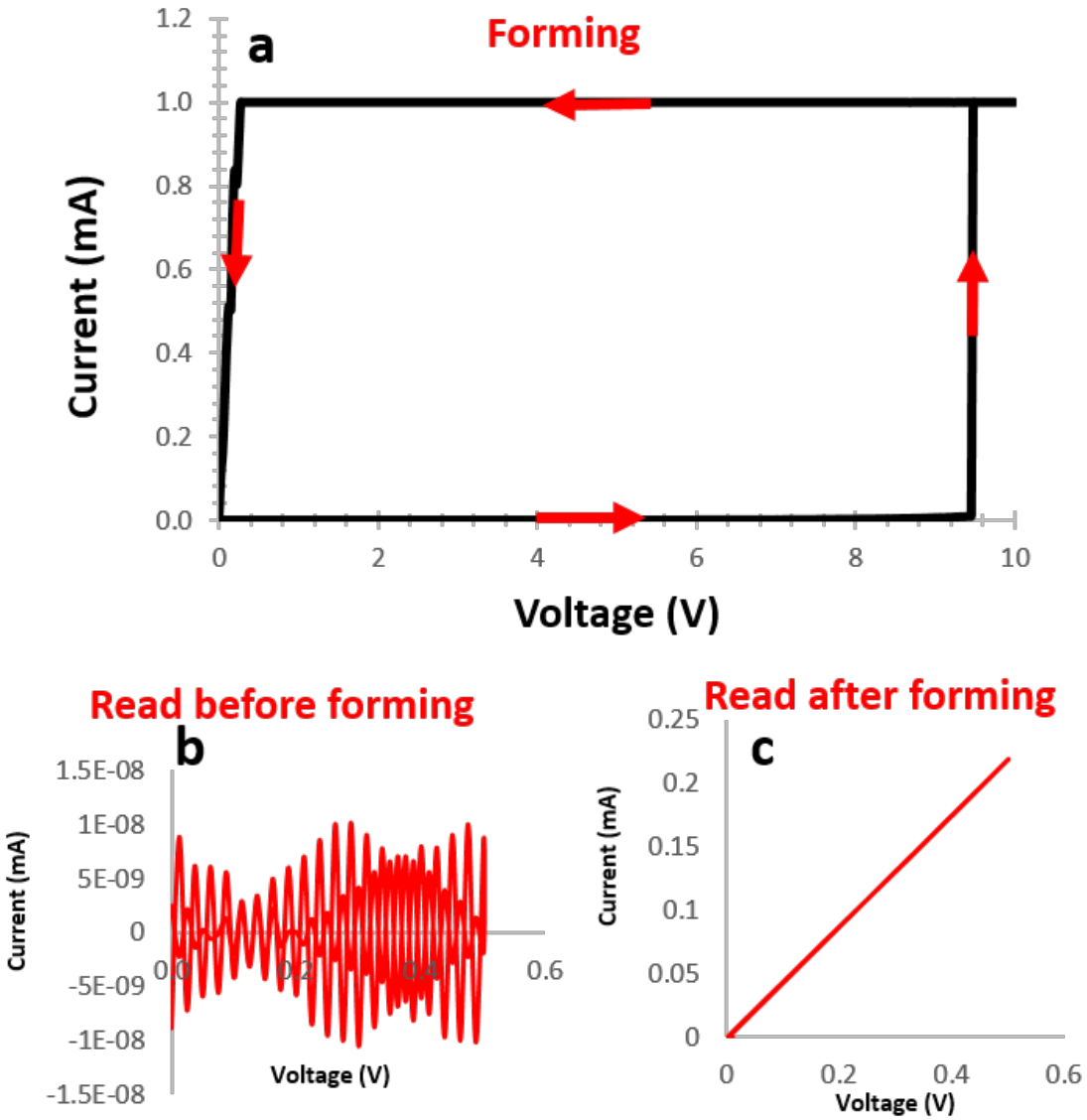

Figure 9. (a) Forming process of rutile titania. (b) read voltage before and (c) read after forming step. (Thickness 50nm).

In order to reset the device and disconnect the conductive path, the voltage was applied to 2 V with a higher IC compared to the forming process (7.5 mA), and the device

switched at 1.4 V, at which point the device returned from LRS to HRS (RESET) as shown in **Figure 10 (a)**. The voltage was swept again in positive 6 V, at which point the conductivity increased gradually from 1.5 V until 5.4 V, where the device switched from HRS to LRS (SET) as shown in **Figure 10(b)**.

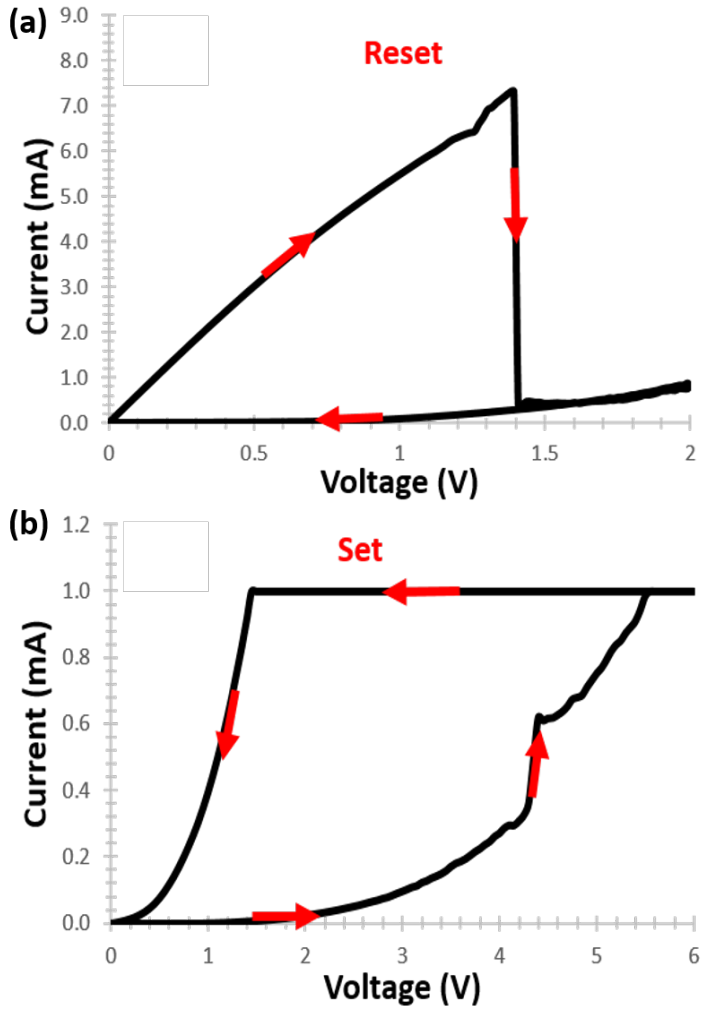

Figure 10. I-V sweeps of unipolar resistive switching behaviour of rutile titania. (a) reset, and (b) set processes. (Thickness 50 nm).

Only the amorphous titania device exhibited bipolar switching behaviour in the Pt/TiO_2/Pt structure. The voltage was swept first to negative (already formed in **Figure 6**) and subsequently to positive polarity. In the device with the amorphous phase of

titania (**Figure. 11**), the device switched at -2.8 V after the SET step (**Figure 6 (b)**) but at a higher IC (10 mA). The RESET process took place at 1.6 V, where the device switched to the HRS once again.

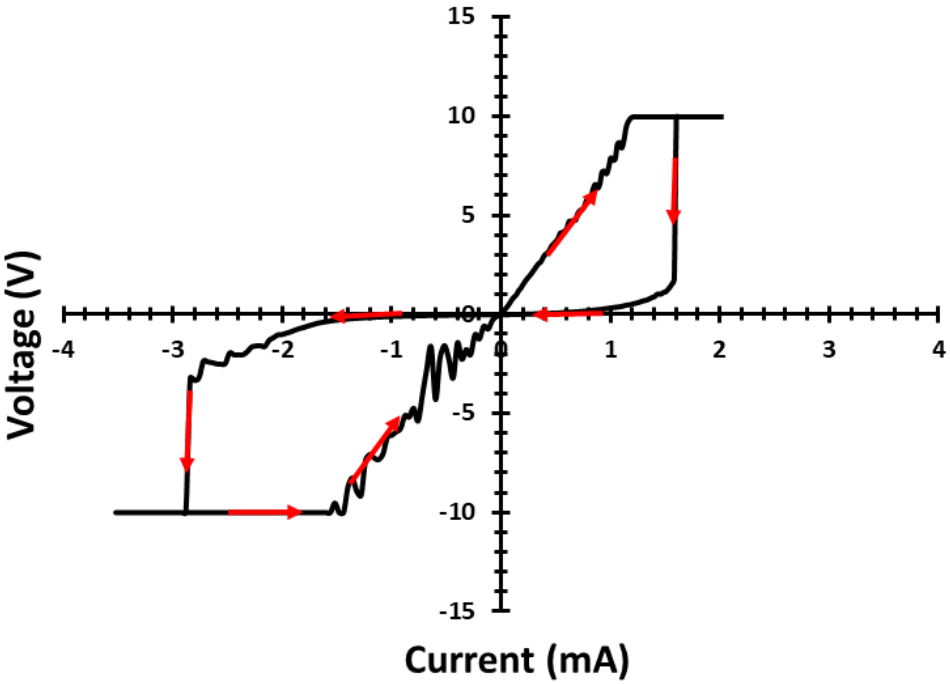

Figure 11. Sweeps of bipolar resistive switching behaviour of amorphous titania with thickness of 50 nm prepared using HT-PVD.

A typical combinatorial library of Pt/TiO_2/Pt devices was evaluated, and the statistics for switching are summarized in **Figure 12**. The switching operation was performed on a number of devices after the forming process with different voltages. The dark blue fields indicate the number of devices that formed successfully. The green fields indicate the number of devices that subsequently, successfully switched in an ReRAM application (reset/set). The number of devices that were tested but failed to work are indicated by white fields. Light blue fields indicate devices that were not tested.

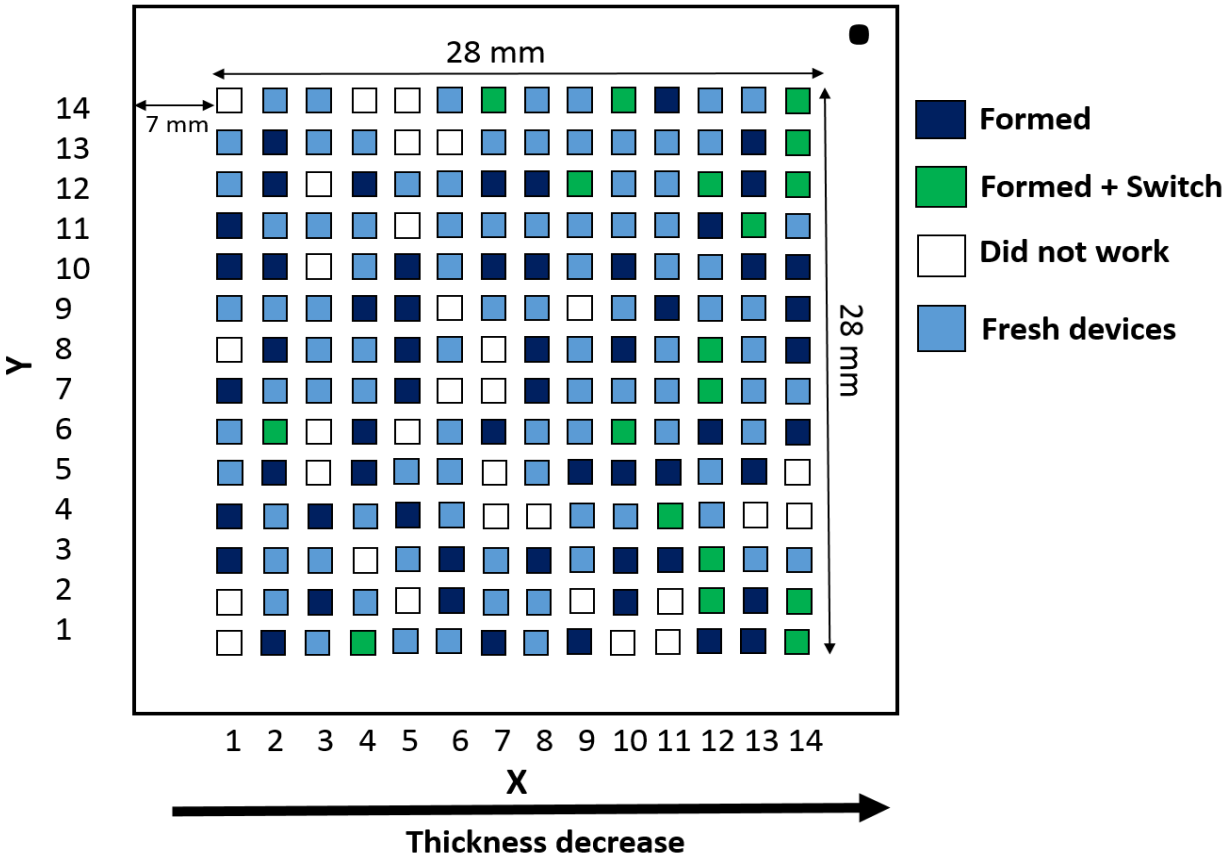

Figure 12. High-throughput statistics of device yields of Pt/TiO_2 amorphous/Pt. Dark blue indicate how many devices were formed; green indicates how many devices were formed and tested and set again; white boxes indicate the number of devices that did not form; and light blue represents devices that were not tested.

By excluding the untested devices and combining all Pt/TiO_2/Pt systems, a clear comparison was achieved, as shown in **Figure 13**. It is important to mention that the data presented here – the data for the thicker devices (200–300 nm) and the thinner devices (10–50 nm) – were combined to give general statistics of device performance. Nearly 140 (red color) devices were formed in the amorphous phase, whereas 130 and 95 devices were formed in the anatase and rutile phases, respectively. The lower number formed in crystalline devices could be due to different densities of defects at which, in addition to

oxygen vacancies, the crystalline grain may play an important role in enhancing the conductivity of the device and thereby leading to its failure. This depends on the switching region at which the grain boundaries of the device should be formed at lower voltage; switching in the middle of forming requires higher voltage. The forming process is one critical success factor for ReRAM application, as the subsequent switching cycle depends on it. However, the subsequent cycle (reset/set) was performed on the devices that already formed. Pt/TiO_2 (all phases)/Pt showed the device performance (blue color). The number of cycled devices for all phases was nearly the same (average of 25 devices). It is important to note that not all formed devices were cycled, since the focus was mainly on the forming process, a critical factor for the switching cycles. The number of devices that did not work (DNW) are indicated (green).

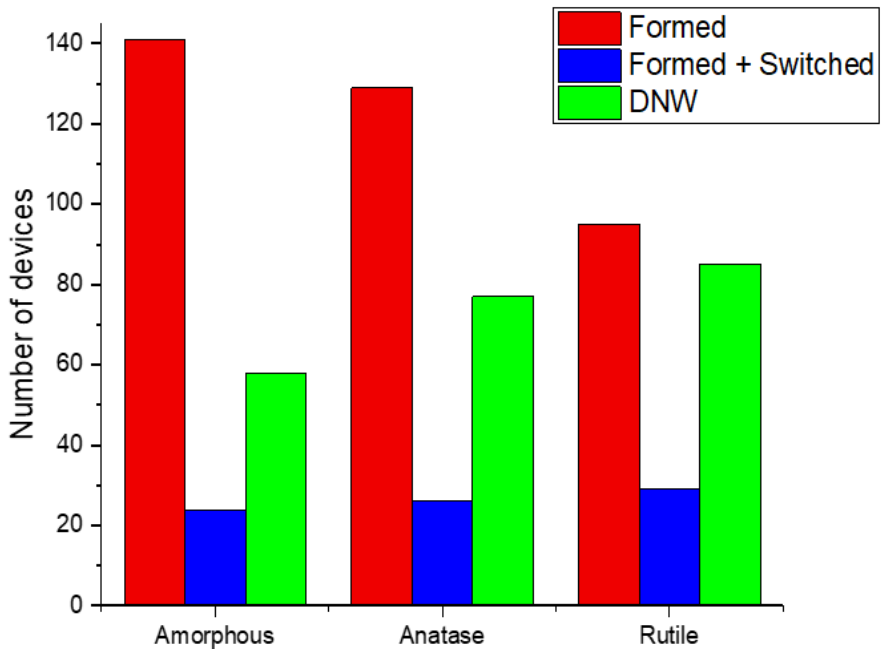

Figure 13. High-throughput statistics of device yields of all Pt/TiO_2/Pt-synthesised systems: a red colour indicates the number of devices formed; blue indicates the number of devices being switched; and green indicates the number of devices that did not work (DNW).

Multiple switching on one device (device No (9, 12)) across different behaviors was performed and is displayed in **Figure 14**. It is clear that the forming process requires higher voltage to create a conductive path through the oxide. The device exhibited much lower voltage in the subsequent cycle. After that, there was nearly stable switching until cycle 15, where the behavior started changing and looked like a unipolar occurrence. On the 28th switching cycle, the hysteresis loop was not observed, and the device became very conductive. This could be due to an O atom becoming excited and leaving an O_2 poor film, resulting in increasing conductivity.

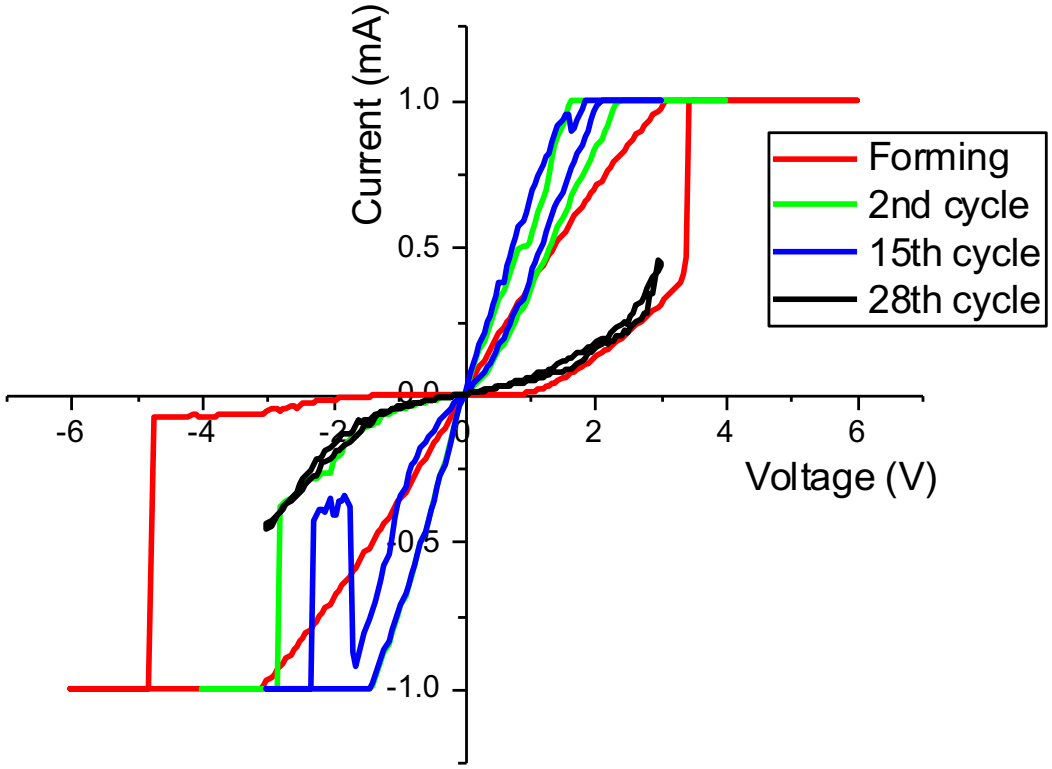

Figure 14. Multiple bipolar switching of Pt/TiO_2 (amorphous)/Pt. Forming (red), 2nd cycle (green), 15th cycle (blue) and 28th cycle (black).

Amorphous titania shows no dependency on forming voltage, whereas crystalline titania (anatase and rutile) shows slight dependency. By calculating the field

of the device, it was found that all phases showed dependency on the field, which decreased with increasing thickness of the devices. The crystalline phases showed higher fields than the amorphous phase. Statistics of all devices showed that most of the devices tested formed successfully with a variation of voltage. This variation was due to different densities of defects. Multiple switching showed that the device lost oxygen with the time of the switching cycle.

3.3. ReRAM Mechanisms

Generally, there are two dominant types of defects suggested to be responsible for the formation of the conducting path, namely titanium interstitials and oxygen vacancies. Marucco et al. [28] reported that the dominating defect of TiO_2 appears thermodynamically controlled, and at a lower temperature, oxygen vacancies are the likely dominating defect. Only at a high temperature will titanium interstitials dominate. Even if the oxygen vacancy defect in TiO_2 is thermodynamically favored, there is a certain upper limit of concentration of these defects that can be accommodated in TiO_2 if its crystal structure is to be sustained [29]. Once the concentration of oxygen vacancies crosses the upper limit, the phase instability of the original TiO_2 structure becomes high, which might lead to phase transition (Magneli phase). Oxygen vacancies serve as donors in TiO_2, which means an increase in their concentration, resulting in an increase in the concentration of delocalized electrons; therefore, the conductivity of the electrical insulator titania will increase. Rutile has received great interest as a strong candidate for

ReRAM applications because it has the highest value for the dielectric constant among the titania phases.[30, 31] The high value of the dielectric constant comes from the highly effective charges of Ti and O ions and the soft optical phonon mode in the crystal structure.[32] However, there are many other properties of the phases, such as point defect and grain boundaries, which may strongly influence the effectiveness of the phase as a reversible switch. Hence, these properties also play a role in determining the forming voltage.

Forming Step (HRS — LRS)

The underlying mechanism of switching in a device can be inferred from characteristic switching behaviour and variations in device construction, such as thickness and the active switching layer. The forming process plays an important role in changing electrical conductivity, oxygen ion migration and physical deformation, which influences the subsequent resistive switching characteristics. The forming process is a partial breakdown of the material. During the forming process, a conducting path forms as a 'soft' (or partial) breakdown in the dielectric material, with oxygen vacancies introduced in the TiO_2 that result in a reduced conducting phase. Joule heating is a voltage-induced thermal dielectric breakdown process enhanced by moving oxygen from an equilibrium state to a non-equilibrium state that causes excessive power dissipation [33]. It is well established that Joule heating is proportional to resistance and increases as the square of the current [34]. Thus, at high IC, memory performance might

be affected due to large heat generation. For this reason, in this work, the IC was as low as 1 mA in all devices in the initial pristine state. The accumulation of oxygen vacancies inside the TiO_2 layer forms a conducting path that connects two separate electrodes, which eventually initiate this transition. There are studies in the literature which have experimentally identified that the conductive filament in TiO_2 is composed of the so-called Magneli phase Ti_nO_{2n-1}. [35 - 37]. It can be assumed that the Magneli phase is responsible for forming the filament [38 - 39]. To form the initial filament (conducting bridge) comprising the Magneli phase, a large concentration of oxygen vacancies must be generated in the oxide in the FS, as shown in **Figure 15,** at which stoichiometric TiO_2 is reduced to sub-stoichiometric TiO_{2-x} and the conductive path is created. Even though a lower IC was applied (1 mA), physical deformation during the forming process was observed, which might be due to oxygen gas evolution. The same observation was reported by Yang et al [40]. The energy needed in the thermochemical reaction is provided by Joule heating from the flowing current (**Figure 5(a), 7(a) and 9(a)**) for amorphous, anatase and rutile, respectively. The conduction of HRS in all phases of $Pt/TiO_2/Pt$ structures shows thermally activated behaviour that suggests filament-type resistive switching as already reported [41-43].

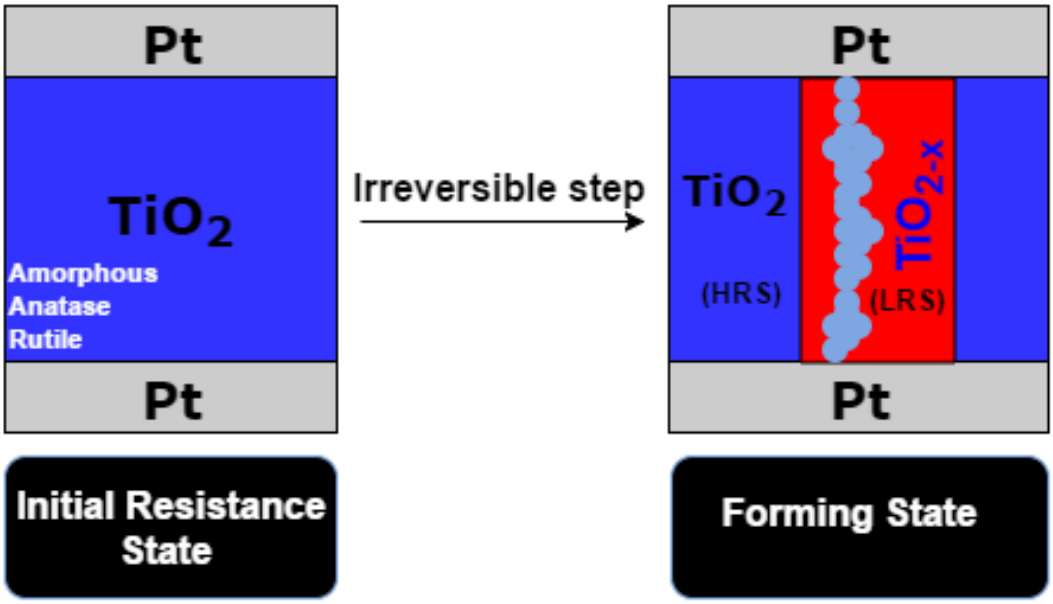

Figure 15. Diagram presenting the forming process and creation of conductive path of Pt/ TiO_2/ Pt structures.

RESET Step (LRS ─ HRS)

One detail of the RESET mechanism is still unclear: It requires higher current each time to RESET the device [44, 45]. However, it can be suggested that RESET could be attributed to local power dissipation due to high current density in the conductive path, where power dissipation induces high temperature in the conductive path, causing either the diffusion of vacancies out of the path or the diffusion of other impurities into the path, or even phase transition [36]. Therefore, the locally ruptured part of the conductive channel becomes insulating so that the overall resistance of the channel increases. This ruptured part may consist of a more insulating phase, the formation of which is again thermally activated through localized Joule heating [46]. A thermally induced redox process near the interface between the metal electrode and the oxide (**Figure 16**) is widely accepted and reported as the mechanism behind the formation and

rupture of the conductive filaments [36, 43]. The resistance of the RESET state is generally much lower than that of the pristine sample but is still far higher than that of the SET state. The promising aspect of this model (filamentary type) is that it does not require the unidirectional motion of oxygen ions during repeated set/reset switching. The material simply changes its phase from metallic (or highly conductive semiconducting) magneli to less conducting defective TiO_{2-x}. In this symmetric binary system, as the electrode material is inert, it could be assumed that oxygen vacancies diffuse out the conductive path due to Joule heating, at which point an oxygen atom diffuses into the conductive path and is exchanged with an oxygen vacancy, which therefore decreases the conductivity of the system; meanwhile, resistance is significantly increased due to the diffusion of oxygen atoms, which would be the major factor for switching from the ON state to the OFF state. It was reported that it does not matter how many oxygen vacancies are needed for reset: Only one oxygen vacancy exchanged with one oxygen atom would be enough to change the state of the device [47].

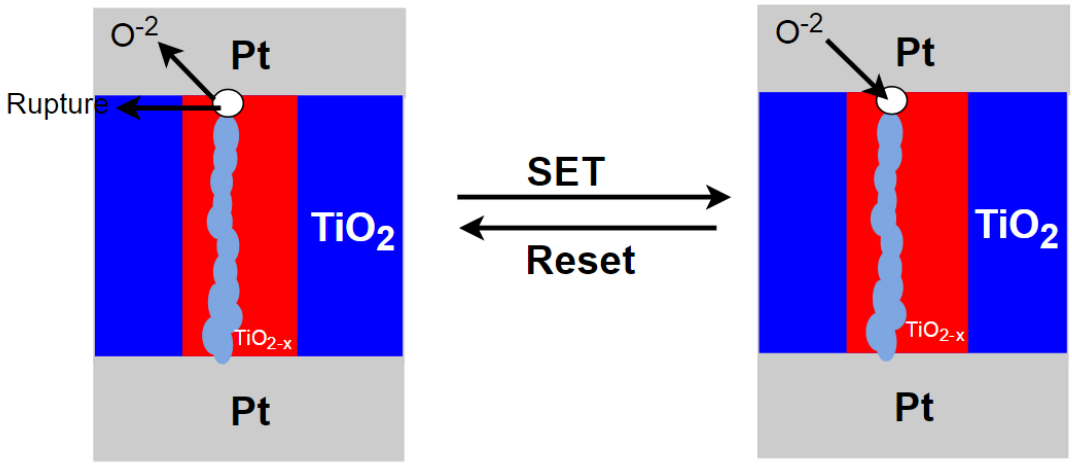

Figure 16. Diagram presenting RESET and SET process of $Pt/TiO_2/Pt$ structures.

SET Step (HRS ─ LRS)

In the RESET process described, localized heat is suggested to occur in the RESET step; and in the subsequent cooling, recrystallization in a more oxygen stoichiometric anatase or rutile phase takes place [48]. This process is propagated by the adjacent crystalline phase around the filament. These re-formed (set process), defective anatase or rutile phases will likely have greater electrical conductivity than pristine stoichiometric TiO_2 for amorphous, anatase and rutile, respectively. However, it still has higher electrical resistance than the Magneli phase.

All the mechanisms mentioned above focused on the unipolar switching mode; bipolar behaviour was observed only on amorphous titania, as described earlier in **Figure 11.** The mechanism here was considered to be due to the electronic or ionic effect, in which electronic and ion migration play an important role in this type of switching. When a substantial Schottky potential barrier is present at the Pt/TiO_2 interface, electronic/ionic bipolar resistive switching (BRS) occurs, which lowers the Schottky barrier due to the low oxygen vacancy concentration near the electrode. Jeong et al. [49] have reported that an increase in the concentration of oxygen vacancies leads to a decrease in the Schottky barrier height at the Pt/TiO_2 interface [50- 51]. Sawa et al [36] reported that the filament was due to the localized drift of oxygen vacancies. It was also found that localized drifting of oxygen vacancies along the direction of the electric field is highly likely to occur with favorable defect migration pathways, such as grain

boundaries [32]. The result obtained suggests that the RESET process is due to ruptured filaments (**Figure 16**) when reversed voltage is applied to the device.

It was reported that [34] stable resistive switching is due to the formation of the crystalline TiO_2 layer, but such annealing can modify the barrier highest at the Pt/TiO_2 interface [52], causing unreliable switching performance; as the temperature increased, the grain size increased, and therefore the current path through the grain boundary became unstable, as found by Kim et al.[52] They found that upon crystallization at high annealing temperatures, the titania exhibited only unipolar behaviour. On deposited titania (most likely to be amorphous), bipolar switching was observed.

It was observed that thinner devices required higher voltage and therefore a higher electrical field. This could be explained by a lower density of defect, which requires higher voltage. It was also observed that the distribution of forming voltage and the electrical field of thicker devices ($D > 150$ nm) was stable as compared to the random distribution of thinner devices ($D \leq 60$ nm). This could be due to the defect size and the physical region of switching: In the case of the thinner device, the defect size was small, which in turn provided a variety of forming voltage. In an amorphous material (in general), there is no band structure. Nevertheless, notions such as 'band gap' or 'band structure' are still applied, but in a broader sense, as compared to crystalline materials. The forming voltage of amorphous was less affected by thickness, which might be due to the point defect presented in amorphous titania. Whereas in crystalline (anatase and rutile), the forming voltage mostly depended on thickness. This, again, depends on the

physical region of switching: In crystalline, both the point defect and grain boundaries were presented. If the switching region is on the boundaries of the grain, the voltage will be low. On the other hand, if the switching region is far from the boundaries, then the voltage will be higher. This could explain why higher voltage is required in anatase and rutile.

4. CONCLUSIONS

High-throughput evaporative PVD has been used to prepare amorphous, anatase and rutile phases of titania on $Si/SiO_2/TiO_2/Pt$ substrates, and characterized with Raman spectroscopy. Electrical characterization of capacitor type model ReRAM structures (Pt top electrode) of the $Pt/TiO_2/Pt$ device was performed. The forming field for a switchable unipolar device was found to be greatest on rutile and lowest on the amorphous phase. However, the resistive contrast was greatest on the rutile phase and lowest on the anatase phase.

ACKNOWLEDGEMENTS

Deanship of Scientific Research of Najran University has supported this work. Project number: NU/ESCI/16/005.Thanks to Professor Brian E. Hayden in University of Southampton, UK.

REFERENCES

1. G. Vidyut, H. Imran H, R. J. Higuchi, R. A. Huertas, H. Pham and Y. Wang, "Less methods and vehicles for high productivity combinatorial testing of materials for resistive random access memory cells," US, (2014).

2. E. Robert, G. Samuel, H. Brian and P. Graeme, "High throughput synthesis and screening of chalcogenide materials for data storage," in International Chemistry Conference Singapore (2005).

3. W. Rainer, S. Georgi and S. Kristof, "Redox-based resistive switching memories nanoionic mechanisms, prospects, and challenges," *Advanced Materials,*. **21**, 2632-2663, (2009).

4. W. Wei and W. Simon W, "RESET Mechanism of TiOx Resistance-Change Memory Device," *IEEE electronic device letters,*. **30**, 333-337, (2009).

5. D. S. Jeong, R. Thomas,R. S. Katiyar and J. F. Scott "Overview on the Resistive Switching in TiO2 Solid Electrolyte," *J. Integrated. Ferroelectrics*, **124**, 87-96, (2011).

6. S. Mojarad, "Leakage current and resistive switching mechanisms in $SrTiO_3$," Electrical and Electronic Engineering, Theses.ncl.ac.uk., (2013).

7. M. Blanka, G. Seong, D. Hyung and N. Yoshio, "Resistive switching mechanisms in random access memory devices incorporating transition metal oxides: TiO_2, NiO and $Pr0.7Ca0.3MnO_3$," *Nanotechnology*, 22 (25):254029, (2011).

8. C. Isotta, D. Jon, M. Claire, V. Audrey and H. Brian,"Innovative catalyst supports to address fuel cell stack durability," *Science direct,*. **38**, 640-645, (2013).

9. Beck, A.; Bednorz, J.; Gerber, C.; Rossel, C.; Widme, D. Reproducible Switching Effect in Thin Oxide Films for Memory Applications. *Appl. Phys. Lett.* **2000**, *77*, 139-141.

10. Yoshida, C.; Tsunoda, K.T.; Noshiro, H.; Sugiyama, Y. High Speed Resistive Switching in Pt/TiO_2/TiN Film for Nonvolatile Memory Application. *Appl. Phys. Lett.* **2007**, *91*, 223510.

11. Yoshida, C.; Kinoshita, K.; Yamasaki, T.; Sugiyama, Y. Direct Observation of Oxygen Movement during Resistance Switching in NiO/Pt Film. *Appl. Phys. Lett.* **2008**, *93*, 042106.

12. Lanza, M. A Review on Resistive Switching in High-k Dielectrics: A Nanoscale Point of View Using Conductive Atomic Force Microscope. *Materials* **2014,** *7*, 2155-2182.

13. Bousoulas, P.; Giannopoulos, J.; Giannakopoulos, K.; Dimitrakis, P.; Tsoukalas, D. Memory Programming of TiO_{2-x} Films by Conductive Atomic Force Microscopy Evidencing Filamentary Resistive Switching. *Appl. Surf. Sci.* **2015**, *332*, 55-61.

14. Do, Y.; Kwak, J.; Bae, Y.; Jung, K.; Im, H.; Hong, J. Hysteretic Bipolar Resistive Switching Characteristics in TiO_2 /TiO_{2-x} Multilayer Homojunctions. *Appl. Phys. Lett.* **2009,** *95*, 093507.

15. Magyari, B.; Tendulkar, M.; Park, S.; Lee, H.; Nishi, Y. Resistive Switching Mechanisms in Random Access Memory Devices Incorporating Transition Metal Oxides: TiO_2, NiO and $Pr_{0.7}Ca_{0.3}MnO_3$. *Nanotechnology* **2011**, *20*, 254029.

16. Rohde, C.; Choi, B.; Jeong, D.; Choi, S.; Zhao, J.; Hwang, C. Identification of a Determining Parameter for Resistive Switching of TiO_2 Thin Films. *Appl. Phys. Lett.* **2005,** *86*, 262907.

17. Kim, S.; Choi, Y. A Comprehensive Study of the Resistive Switching Mechanism in Al/TiO_x/TiO_2/Al-Structured RRAM. *IEEE Trans. Electron Devices* **2009,** *56*, 3049-3053.

18. Schiavello, M. *Heterogeneous Photocatalysis*. John Wiley and Sons: **1997**.

19. Hayden, B.; Pletcher, P.; Suchsland, J.; Williams, L. The Influence of Support and Particle Size on the Platinum Catalysed Oxygen Reduction Reaction. *Phys. Chem.* **2009,** *11*, 9141-9148.

20. Suchsland, J.; Hayden, B. Partical Size and Substrate Effect in Electrocatalysis. Ph.D. Dissertation, Southampton University, **2007**.

21. G. Samual and H. Brian, "Physical vapor deposition method for the high-throughput synthesis of solid-state material libraries," *Comb. Chem,*. **8**, 66-73, (2006).

22. S. Castrejon and L. M. Camacho, "Quantification of phase content in TiO2 thin films by Raman spectroscopy," *Sociedad Mexicana de Ciencia y Tecnología de Superficies y Materiales,*. **27**, 88-92, (2014).

23. T. Mazza, E. Barborini, P. Piseri, P. Milani, D. Cattaneo, A. Li Bassi, C. E. Bottani, and C. Ducati, "Raman spectroscopy characterization of TiO2 rutile nanocrystals, *Phys. Rev*. B,. **75**, 045416, (2007).

24. Wypych, A.; Bobowska, I.; Tracz, M.; Opasinska, A.; Kadlubowski, S.; Kaliszewska, A.; Grobelny, J.; Wojciechowski, P. Dielectric Properties and Characterisation of Titanium Dioxide Obtained by Different Chemistry Methods. J. Nanomater. 2014, 9, 124814.

25. K. Kim, G. Song, J. Seok, M. Lee, J. Yoon and C. Hwang, "Electrically configurable electroforming and bipolar resistive switching in Pt/TiO2/Pt structures. *Nanotechnology,*. **21**, 305203, (2010).

26. G. Marlasca, N. Ghenzi, M. Rozenberg and P. Levy, "Understanding electroforming in bipolar resistive switching oxides. *Appl. Phys Lett,*. **98**. 042901, (2011).

27. J. Strachan, J. Yang, A. Montoro, A. Ospina, A. Ramirez, A. Kilcoyne, G. Ribeiro and S. Williams, S. Characterization of electroforming-free titanium dioxide memristors. *Nanotechnology,*. **4**, 467-473, (2013).

28. K. M. Kim, G. H. Kim, S. J. Song, J. Y. Seok, M. H. Lee, J. H. Yoon and C. S. Hwang, "Electrically configurable electroforming and bipolar resistive switching in Pt/TiO2/Pt structures," *Nanotechnology,*. **21**, 305203, (2010).

29. K. T. Chikako Yoshida, H. Noshiro and Y. Sugiyama, "High speed resistive switching in Pt TiO_2 Ti N film for nonvolatile memory application," *Applied physics letters,*. **91** (22), 223510, (2007).

30. J. Marucco, P. Lemasson and j. Gautron, "Thermogravimetric and electrical study of nonstoichiometric titanium dioxide TiO2−x, between 800 and 1100°C", *J. Phys. Chem. Solids,*. **42** (5), 363-367, 1981.

31. A. Stoneham and W. Hayes, "*Defect and Defect Process in Nonmetallic Solids*", Wiley: New York, (1985).

32. J. Yang, J. Strachan, F. Miao, M. Zhang, M. Pickett, W. Ti, D. Ohlberg, M. Riberiro and R. Williams, "Metal/TiO_2 interfaces for memristive switches",. *Appl. Phys*,. **102**, 785789, (2011).

33. U. Diebold, "The Surface Science of Titanium Dioxide", *Surf. Sci. Rep*,. **48**, 53-229, (2003).

34. D. Acharyya, A. Hazra, P. Bhattacharyya, "A journey towards reliability improvement of TiO_2 based resistive random access memory", *Rev. Microelec*,. **54**, 541-560, (2014).

35. M. Siddik, S. Jung, W. Lee, J. Shin, S. Park, D. Lee, I. Kim and H. Hwang, "Thermally assisted resistive switching in $Pr0.7Ca0.3MnO_3$/Ti/$Ge_2Sb_2Te_5$ stack for nonvolatile memory applications", *Appl. Phys*,. **99**, 063501, 2011.

36. A. Sawa, "Resistive switching in transition metal oxides", *Mater. Today*,. 11(6), 28-36, 2008.

37. S. Kelly, F. Polak and M. Tomkiewicz, "Raman spectroscopy as a morphological probe for TiO2 aerogels", *Phys. Chem*,. **101**, 2730 – 2734, (1997).

38. D. Lelmini, R. Bruchhaus and R. Waser, "Thermochemical resistive switching: materials, mechanisms, and scaling projections", Phase. *Transitions*,. 84 (7), 570-602, (2011).

39. D. Jeong, R. Thomas, R. Katiyar, and J. Scott, "Overview on the Resistive switching in TiO2 solid electrolyte", *Korea Institute of Science and Technology*,. 2011, 124, 87-96, (2011).

40. R. Waser, R. D. Dittmann, G. Staikov and K. Szot, "Prospects and challenges of redox-based RRAM concepts", *IMEC*: (2008).

41. J. Yang, F. Miao, M. Pickett, D. Ohlberg, D. Stewart, C. Lau and R. Williams, "The Mechanism of electroforming of metal oxide memristive switches," *Nanotechnology*,. 20, 215201, (2009).

42. H. Akinaga and H. Shima, "Resistive random access memory (ReRAM) Based on metal oxides. proceedings of nanodevice innovation conference, Japan: *IEEE*, (2010).

43. S. Hisashiand, A. Hiroyuki, "Basics of RRAM based on transition metal oxides; nanodevice innovation research center, *International Symposium on Advanced Gate Stack Technology*, (2010).

44. H. Akinaga, "Recent Advance and Prospects in ReRAM Technology," *Sematech Symposium*, Japan, 2011.

45. C. Rohde, B. Choi, D. Jeong, S. Choi, J. Zhao and C. Hwang, "Identification of a determining parameter for resistive switching of TiO2 thin films," *Appl. Phys. Lett*,. **86**, 262907, (2005).

46. W. Wang, S. Fujita and S. Wong," RESET mechanism of TiOx resistance-change memory device. *IEEE Electron Device Lett*,. **30**, 733-735, (2009).

47. D. S. Jeong, "Resistive switching in Pt/TiO2/Pt. Ph.D. *Dissertation. Aachen University*, Germany, (2008).

36. R. H Austin and S. F .Lim, "The sackler colloquium on promises and perils in nanotechnology for medicine," *Proceedings of the National Academy of Sciences*,. 105 (45), 1721717221, (2008).

48. K. Yoon, M. Lee, G. Kim, S. Song, J. Seok,,S. Han, S, H. Yoon, K. Kim and C. Hwang, "Memristive Tri-stable resistive switching at ruptured conducting filaments of a Pt/TiO2/Pt cell", *Nanotechnology.,* **23**, 185202, (2012).

49. D. Jeong, H. Schroeder and R. Waser," Mechanism for bipolar Switching in a Pt/TiO2/Pt resistive switching cell", *Phys. Rev,.* **79**, 195317, (2009).

50. K. Kim, B. Choi, Y. Shin, S. Choi and Hwang, C. anode-interface localized filamentary mechanism in resistive switching of TiO_2 thin films", *Appl. Phys. Lett*. **91**, 012907, (2007).

51. K. Kinoshita, T. Tamura, M. Aoki, Y. Sugiyama and H. Tanaka, "Bias polarity dependent data retention of resistive random access memory consisting of binary transition metal oxide", *Appl. Phys. Lett*. **89**, 103509. (2006).

52. W. Kim and S. Rhee, "Effect of the top electrode material on the resistive switching of TiO_2 thin film", *Microelectron Engg,.* **87** (2), 98-103, (2010).